Virologica Sinica 40 (2025) 822–834

Contents lists available at ScienceDirect

Virologica Sinica

journal homepage: www.keaipublishing.com/en/journals/virologica-sinica
www.virosin.org

Research Article

African swine fever virus MGF360-9L degrades DDX20 through the Rab1A-dependent autophagy pathway to antagonize its antiviral effect

Lu He [a,b,c,1], Xuxu Fan [a,b,c,1], Zhaoyu Zhu [a,b,c], Danshi Pei [a,b,c], Yizhuo Wang [a,b,c], Xizhong Li [a,b,c], Qingfeng Ren [a,b,c], Haixue Zheng [a,b,c,*], Weiwei Li [a,b,c,*], Zixiang Zhu [a,b,c,*]

[a] State Key Laboratory for Animal Disease Control and Prevention, College of Veterinary Medicine, Lanzhou University, Lanzhou Veterinary Research Institute, Chinese Academy of Agricultural Sciences, Lanzhou 730000, China
[b] African Swine Fever Regional Laboratory of China, Lanzhou Veterinary Research Institute, Chinese Academy of Agricultural Sciences, Lanzhou 730046, China
[c] Gansu Province Research Center for Basic Disciplines of Pathogen Biology, Lanzhou 730046, China

ARTICLE INFO

Keywords:
African swine fever virus (ASFV)
MGF360-9L
DDX20
Rab1A
Protein degradation
Autophagy

ABSTRACT

African swine fever (ASF) is an acute, hemorrhagic, and highly contagious disease in pigs caused by the African swine fever virus (ASFV). Our previous studies have demonstrated that deletion of the *MGF360-9L* gene weakens ASFV virulence in pigs, yet the underlying mechanism remains unclear. To investigate the mechanism of MGF360-9L regulating ASFV pathogenicity, the relationship between MGF360-9L and host proteins was identified by mass spectrometry. We found that host protein DEAD-box helicase 20 (DDX20) interacted with and colocalized with MGF360-9L. Overexpression of DDX20 inhibited ASFV replication, whereas knockdown of DDX20 had the opposite effects. Moreover, DDX20 inhibited ASFV replication by promoting the activation of type I interferon signaling. Surprisingly, DDX20 was gradually degraded following ASFV infection. Mechanistically, MGF360-9L promoted the autophagic degradation of DDX20 by recruiting autophagy-related protein Ras-related protein Rab-1A (Rab1A). Silencing Rab1A suppressed ASFV replication, while overexpression of Rab1A exhibited the opposite effects. Furthermore, Rab1A, MGF360-9L and DDX20 could form a complex to facilitate the degradation of DDX20. Knockdown of Rab1A impaired MGF360-9L-mediated degradation of DDX20 during ASFV infection. In summary, our study demonstrates that MGF360-9L targets DDX20 for autophagy degradation to antagonize its antiviral function and facilitate ASFV replication. This finding broadens our understanding of the regulatory network between ASFV and its host, and provides new insights into the pathogenesis and immune evasion mechanisms of ASFV.

INTRODUCTION

African swine fever (ASF) is a highly pathogenic infectious disease caused by the African swine fever virus (ASFV). The disease is highly contagious among domestic pigs and wild boars, with a mortality rate of nearly 100% (Wang et al., 2021). Since the first outbreak in Kenya in the 1920s, ASF has been reported across Africa, Europe and the Americas over the past century (Alejo et al., 2003). In 2018, the disease was first detected in northeastern China and subsequently spread rapidly throughout the country, resulting in significant economic losses (Zhou et al., 2018). ASFV is an enveloped double-stranded DNA virus and the only member of the *Asfivirus* genus of the *Asfarviridae* family (Huang et al., 2023). It possesses a large genome, ranging from 170 to 190 kb, and contains over 150 open reading frames (ORFs) that encode more than 50 structural proteins as well as more than 100 non-structural proteins (De Villiers et al., 2010; Karger et al., 2019). Despite some virulence factors of ASFV have been identified, how these virulence factors regulate viral replication remains largely unknown.

The complete ASFV genome comprises a central conserved region of approximately 100 kb, along with a left variable region (LVR) of about 45 kb and a right variable region (RVR) of approximately 25 kb. The LVR and RVR regions of the ASFV genome are important, as they contain five

* Corresponding authors.
E-mail addresses: haixuezheng@163.com (H. Zheng), liweiwei@caas.cn (W. Li), zhuzixiang@caas.cn (Z. Zhu).
[1] Lu He and Xuxu Fan contributed equally to this work.

https://doi.org/10.1016/j.virs.2025.10.001
Received 15 April 2025; Accepted 13 October 2025
Available online 14 October 2025

multigene families (MGFs). Although the proteins encoded by MGFs are not essential for viral replication *in vitro*, they have been demonstrated to play crucial roles in viral pathogenicity, host range, and immune regulation (Zsak et al., 2001; Reis et al., 2017; Rathakrishnan et al., 2022). In recent years, MGFs of ASFV, including MGF360, MGF505 and MGF530, have been extensively studied and reported to play crucial roles in the life cycle of ASFV. Studies have shown that ASFV strains with MGF360 and MGF505 deficiency exhibit attenuated virulence in pigs and reduced apoptosis in porcine alveolar macrophages (PAMs) by inhibiting the nuclear factor kappa B (NF-κB) signaling pathway and interleukin 1 beta (IL-1β) mRNA transcription (O'donnell et al., 2015; Gao et al., 2021). In addition, MGF360 and MGF530 not only affect the production of type I interferon (IFN–I) in host cells, but also play a critical role in determining the host cell tropism of ASFV (Yozawa et al., 1994; Afonso et al., 2004). MGF360-9L belongs to the MGF360 family, which is located in the LVR of the ASFV genome and is highly conserved across the viral genome. In our previous study, we demonstrated that ASFV MGF360-9L is a major virulence factor that antagonizes the Janus kinase (JAK)/signal transducer and activator of transcription (STAT) signaling pathway, thereby inhibiting the production of IFN-I (Zhang et al., 2022). The interaction between MGF360-9L and host proteins could provide insights into the pathogenesis of ASFV. Therefore, we constructed the interaction map of MGF360-9L with host proteins using co-immunoprecipitation and liquid chromatography-mass spectrometry. Our analysis revealed that D-E-A-D box helicase 20 (DDX20) was a key component of the map, suggesting that DDX20 interacted with MGF360-9L (Yang et al., 2021).

DDX20 belongs to the D-E-A-D box RNA helicase family. Like other members of the family, DDX20 contains a distinctive Asp-Glu-Ala-Asp (D-E-A-D) sequence motif, which is essential for its helicase activity (Ali, 2021). DDX20 is a multifunctional protein that not only unwinds RNA duplexes, but also participates in RNA binding, RNA metabolism, RNA structural rearrangement and ribonucleoprotein synthesis (Curmi and Cauchi, 2018). Moreover, DDX20 is crucial for the viral life cycle, acting either as a cofactor for the virus or as a regulator of antiviral innate immunity (Ali, 2021). Epstein-Barr virus (EBV) promotes the binding of DDX20 to p53 and blocks the DNA-binding affinity of p53, thereby facilitating EBV-induced cell proliferation and anti-apoptotic activity (Cai et al., 2011). Recent studies have shown that DDX20 can regulate NF-κB and p53 signaling pathways in tumorigenesis and development (He et al., 2023). However, the function of DDX20 in regulating viral replication is not well-defined.

In this study, we found that DDX20 inhibited ASFV replication by activating the IFN-I signaling. Meanwhile, MGF360-9L facilitated the degradation of DDX20 via the autophagy pathway during ASFV infection. Furthermore, we demonstrated that Rab1A, recruited by MGF360-9L, was involved in the degradation of DDX20. Our study reveals a mechanism for the regulation of ASFV replication by the virulence factor MGF360-9L and provides evidence for the important role of MGF360-9L in ASFV pathogenicity.

RESULTS

ASFV MGF360-9L interacts with DDX20

ASFV MGF360-9L is a key virulence factor that may manipulate various cellular signaling pathways to facilitate viral replication. Based on the interaction network of ASFV MGF360-9L with host proteins, we first identified the association between MGF360-9L and DDX20. We co-transfected human embryonic kidney cells (HEK 293T cells) with Flag-MGF360-9L and Myc-DDX20 expression plasmids for exogenous co-immunoprecipitation experiments. The results indicated that MGF360-9L interacted with DDX20 (Fig. 1A and B). Moreover, we transfected porcine kidney cells (PK-15 cells) with Flag-MGF360-9L expression plasmid for semi-endogenous co-immunoprecipitation experiments. Immunoblot analysis showed that MGF360-9L interacted with endogenous DDX20 in PK-15 cells (Fig. 1C). We further investigated whether endogenous DDX20 interacts with MGF360-9L during ASFV infection. PAMs were infected with ASFV-WT (MOI = 1) for 36 h before performing the endogenous co-immunoprecipitation experiments. The results confirmed the interaction between MGF360-9L and DDX20 (Fig. 1D).

As shown in Fig. 1E, GST pull-down assays showed that MGF360-9L directly interacted with DDX20. To analyze the co-localization of DDX20 and MGF360-9L, PK-15 cells were co-transfected with Myc-DDX20 and Flag-MGF360-9L expression plasmids for 24 h before the indirect immunofluorescence assay (IFA) was performed. As shown in Fig. 1F, confocal microscopy revealed that MGF360-9L colocalized with DDX20 in the cytoplasm. Collectively, these results suggest that MGF360-9L is able to interact with DDX20.

DDX20 inhibits ASFV replication

To explore whether DDX20 has an effect on the replication of ASFV, we transfected Myc-DDX20 expression plasmid into *Cercopithecus aethiops* kidney cells (MA104 cells) before ASFV infection. As shown in Fig. 2A, qPCR analysis showed that overexpression of DDX20 inhibited the mRNA level of ASFV *p72* in a dose-dependent manner. Consistently, immunoblot analysis indicated that overexpression of DDX20 inhibited the expression of ASFV structural proteins p72 and p30 in a dose-dependent manner (Fig. 2B). To further investigate the inhibitory effect of DDX20 on ASFV replication, MA104 cells were transfected with Myc-DDX20 expression plasmid for 24 h, and then the cells were infected with ASFV for 12 h, 24 h and 36 h. qPCR analysis indicated that overexpression of DDX20 inhibited the transcription of ASFV *p72* gene during ASFV infection (Fig. 2C). Consistently, as shown in Fig. 2D, overexpression of DDX20 reduced ASFV p72 and p30 expression at different time points after ASFV infection. To investigate whether endogenous DDX20 is involved in ASFV replication, we designed four siRNAs specifically targeting the porcine *DDX20* gene, which down-regulated the transcription and expression of DDX20 to different levels (Fig. 2E and F). Among them, siDDX20-4 showed the best knockdown efficiency. PAMs were transfected with the indicated siRNA for 24 h and then infected with ASFV for 12 h, 24 h and 36 h. As shown in Fig. 2G, qPCR experiments indicated that knockdown of DDX20 enhanced the transcription of *p72* gene in ASFV-infected PAMs. Consistently, knockdown of DDX20 increased the expression of ASFV structural proteins p72 and p30 (Fig. 2H). Taken together, these data suggest that DDX20 inhibits ASFV replication and may be an important host limiting factor in the life cycle of ASFV.

DDX20 inhibits ASFV replication by promoting IFN-I signalling

Since previous study has reported that DDX20 positively regulates the interferon pathway (Chen et al., 2024), we further investigated whether DDX20 inhibits ASFV replication by facilitating the activation of the IFN-I signaling pathway. As shown in Fig. 3A, DDX20 was overexpressed in HEK 293T cells, and the impact of DDX20 on IFN-β reporter activation was assessed using a dual-luciferase assay. The results showed that DDX20 activated the IFN-β reporter in the absence of virus infection (Fig. 3A). Notably, the activation of the IFN-β reporter leads to the upregulation of downstream pro-inflammatory genes and cytokines. As shown in Fig. 3B–D, qPCR analysis indicated that overexpression of DDX20 promoted the transcription of cytokines including *IFNA*, *IFNB1* and *MX1*. We next examined the effect of DDX20 on IFN-β reporter activation upon ASFV infection. MA104 cells were transfected with Myc-DDX20 expression plasmid before ASFV infection to perform reporter assays. As shown in Fig. 3E, overexpression of DDX20 potentiated the activation of the IFN-β reporter upon ASFV infection. Consistently, overexpression of DDX20 promoted the transcription of antiviral genes, including *IFNB1*, *ISG56* and *ISG54,* during ASFV infection (Fig. 3F–H). Collectively, these results suggest that DDX20 promotes the activation of IFN-I signaling, thereby inhibiting ASFV replication.

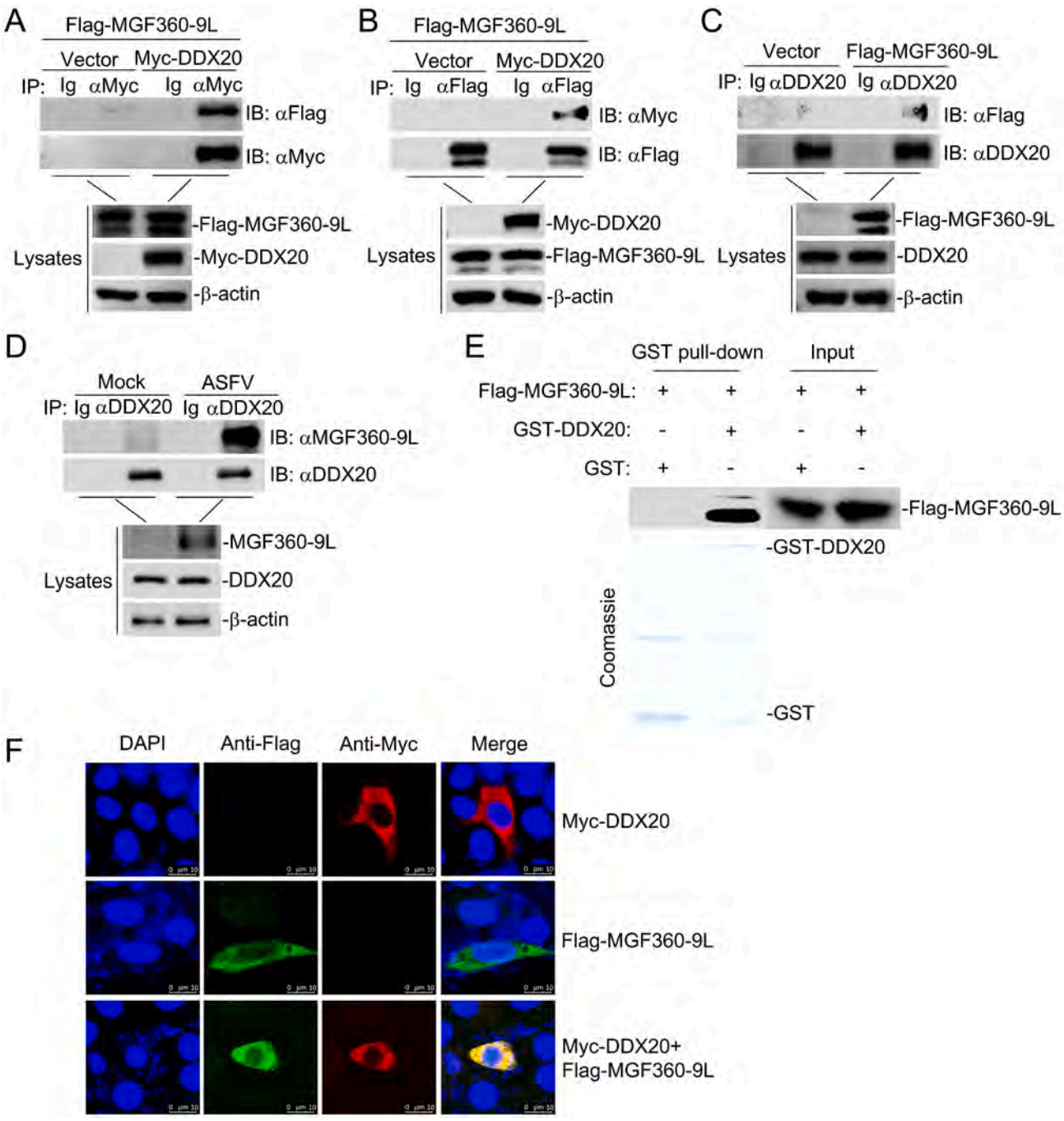

Fig. 1. MGF360-9L interacts with DDX20. **A, B** HEK 293T cells cultured in 10 cm dishes were co-transfected with Flag-MGF360-9L (6 μg/dish) and Myc-DDX20 (6 μg/dish) plasmids for 24 h. Cell lysates were subjected to co-immunoprecipitation with anti-Myc antibody (**A**) or anti-Flag antibody (**B**) and immunoblot assays with the indicated antibodies. **C** PK-15 cells cultured in 10 cm dishes were transfected with Flag-MGF360-9L expression plasmid (6 μg/dish) for 24 h. Cell lysates were subjected to co-immunoprecipitation with anti-DDX20 antibody and immunoblot assays with the indicated antibodies. **D** PAMs were infected with ASFV (MOI = 1) for 36 h. Cell lysates were subjected to co-immunoprecipitation with anti-DDX20 antibody and immunoblot assays with the indicated antibodies. **E** HEK 293T cells cultured in 10 cm dishes were transfected with Flag-MGF360-9L (8 μg/dish) plasmid for 24 h. Purified GST-DDX20 protein coupled to glutathione sepharose beads was incubated with the cell lysates for 3 h at 4 °C and then subjected to GST pull-down assays. The samples were subjected to SDS-PAGE before coomassie blue staining. **F** PK-15 cells cultured in confocal dishes were co-transfected with Flag-MGF360-9L (2 μg/dish) and Myc-DDX20 (2 μg/dish) plasmids for 24 h, immune-staining was performed using specific antibodies against Flag and Myc. Scale bar = 10 μm.

MGF360-9L degrades DDX20 through the autophagy pathway

Given that DDX20 can inhibit ASFV replication, we next aimed to determine whether ASFV antagonizes the antiviral function of DDX20 by modulating its expression to enhance viral replication. PAMs were infected with ASFV (MOI = 0, 0.1, 0.5, 1) for 24 h, and the expression of DDX20 was examined by immunoblot. As shown in Fig. 4A, the expression of endogenous DDX20 was reduced in a dose-dependent manner following ASFV infection. The above results confirmed that MGF360-9L interacted with DDX20; therefore, we wondered whether MGF360-9L was responsible for the degradation of DDX20. To further investigate whether MGF360-9L is involved in the regulation of DDX20 expression, MGF360-9L-deleted ASFV strain (ASFV-ΔMGF360-9L) was obtained and used to infect PAMs for 24 h (Zhang et al., 2022). As shown

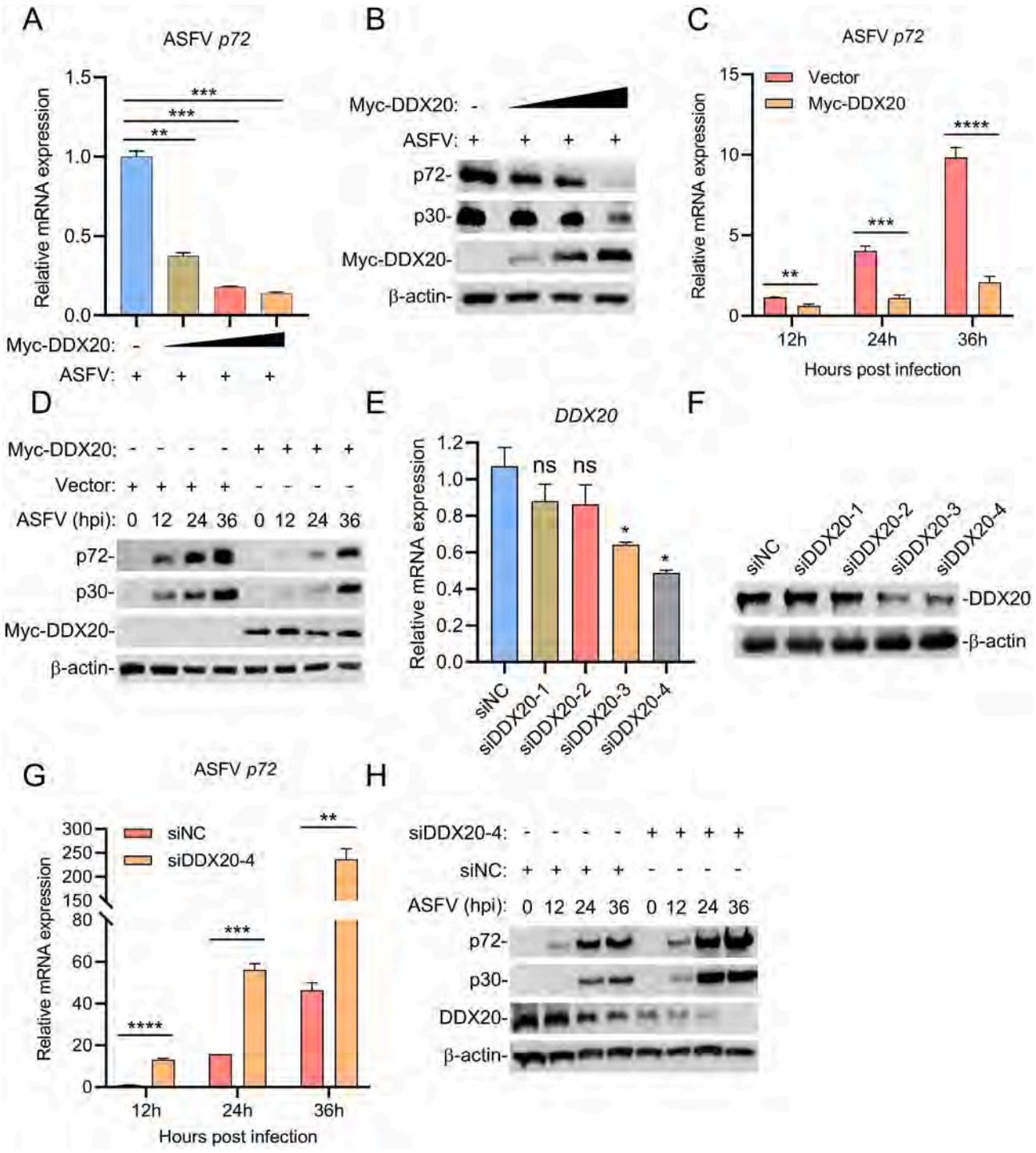

Fig. 2. DDX20 inhibits ASFV replication. **A, B** MA104 cells cultured in 12-well plates were transfected with different amounts of empty vector or Myc-DDX20 (0.5 μg/well, 1 μg/well or 2 μg/well) plasmid for 24 h and then infected with ASFV (MOI = 1) for another 24 h before qPCR assay (**A**) and immunoblot analysis (**B**). **C, D** MA104 cells cultured in 12-well plates were transfected with empty vector or Myc-DDX20 (1 μg/well) plasmid for 24 h. Then the cells were infected with ASFV (MOI = 1) for 12 h, 24 h and 36 h before qPCR experiments (**C**) and immunoblot assays (**D**) were performed. **E, F** PAMs cultured in 12-well plates were transfected with siNC, siDDX20-1, siDDX20-2, siDDX20-3, siDDX20-4 (final concentration, 40 nM) for 24 h before qPCR assays (**E**) or immunoblot assays (**F**). **G, H** PAMs cultured in 12-well plates were transfected with the siDDX20-4 (final concentration, 40 nM). Twenty-four hours later, cells were infected with ASFV (MOI = 1) for 12 h, 24 h and 36 h before qPCR experiments (**G**) or immunoblot assays (**H**). Data were analyzed by unpaired, two-tailed Student's *t*-test. Data are presented as the means ± SDs from three independent experiments. ns $P > 0.05$, *$P < 0.05$, **$P < 0.01$, ***$P < 0.001$, ****$P < 0.0001$.

in Fig. 4B, ASFV-ΔMGF360-9L infection had no marked effects on the expression of DDX20. These results indicated that MGF360-9L is responsible for the expression of DDX20. To further corroborate these findings, PAMs were infected with ASFV and ASFV-ΔMGF360-9L (MOI = 1) for 24 h and 48 h. The results indicated that ASFV infection inhibited DDX20 expression in a time-dependent manner (Fig. 4C). However, ASFV-ΔMGF360-9L infection had no obvious effects on DDX20 expression at 24 h and 48 h (Fig. 4D). The results indicate that MGF360-9L is involved in the degradation of DDX20 upon ASFV infection. We further explored the role of MGF360-9L in DDX20 degradation

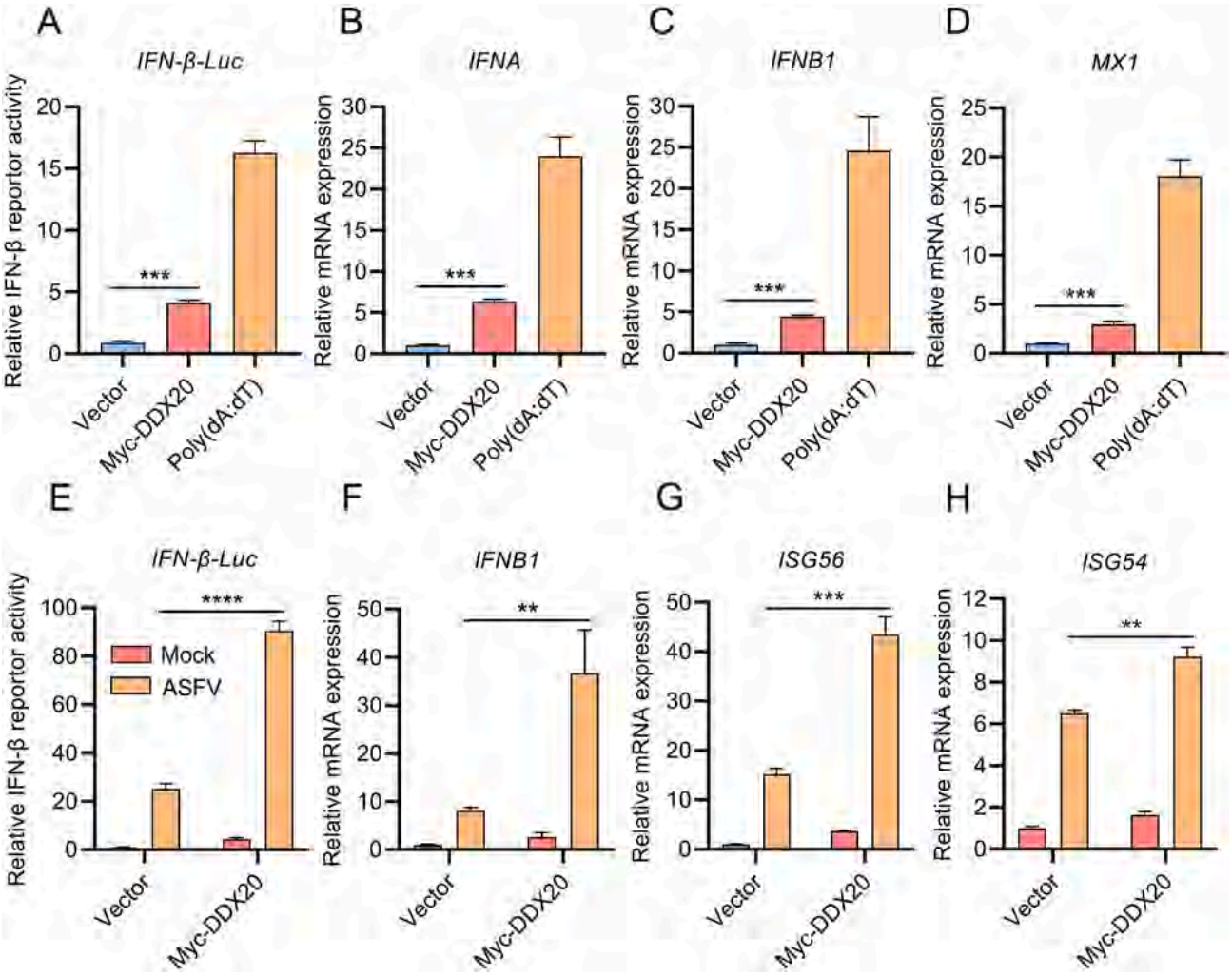

Fig. 3. DDX20 activates the IFN-I signaling pathway to inhibit ASFV replication. **A** MA104 cells cultured in 24-well plates were co-transfected with Vector (1 mg/well) or Myc-DDX20 (1 mg/well) plasmid along with pIFN-b-Luc (200 ng/well) and pRL-TK (100 ng/well) plasmids for 24 h. The cells were then treated with Poly (dA:dT) (20 ng/ml) for 10 h or left untreated before luciferase assays were performed. **B–D** MA104 cells cultured in 12-well plates were transfected with empty vector plasmid (1 μg/well) or Myc-DDX20 plasmid (1 μg/well) for 24 h before qPCR experiments were performed. MA104 cells cultured in 12-well plates and stimulated with Poly (dA:dT) (20 ng/ml) for 10 h were used as the positive control. **E** MA104 cells cultured in 24-well plates were co-transfected with Vector (1 μg/well) or Myc-DDX20 (1 μg/well) along with pIFN-β-Luc (200 ng/well) and pRL-TK (100 ng/well) plasmids. Twenty-four hours later, cells were uninfected or infected with ASFV (MOI = 2) for 30 h before luciferase assays were performed. **F–H** MA104 cells cultured in 24-well plates were transfected with empty vector (1 μg/well) or Myc-DDX20 (1 μg/well) plasmid for 24 h. Then the cells were uninfected or infected with ASFV (MOI = 2) for 30 h before qPCR experiments were performed. Data were analyzed by unpaired, two-tailed Student's *t*-test. Data are presented as the means ± SDs from three independent experiments. $^{**}P < 0.01$, $^{***}P < 0.001$, $^{****}P < 0.0001$.

by overexpressing MGF360-9L in HEK 293T cells. As shown in Fig. 4E and F, MGF360-9L overexpression decreased the expression level of DDX20 in a dose-dependent manner, whereas MGF360-9L overexpression showed little effect on the transcription of the *DDX20* gene.

To investigate the mechanism by which MGF360-9L degrades DDX20, inhibitors targeting different degradation pathways were used in the following experiments. 3-MA and CQ are inhibitors of the early and late stages of autophagy, respectively, while MG132 inhibits the proteasome pathway. HEK 293T cells were co-transfected with an empty vector or Flag-MGF360-9L expression plasmid and Myc-DDX20 expression plasmid. After 18 h, the cells were treated with inhibitors, including 3-MA, CQ and MG132, for 6 h before immunoblot assays. As shown in Fig. 4G, MGF360-9L-mediated degradation of DDX20 was recovered following 3-MA and CQ treatment but remained unchanged in the presence of MG132. Given that 3-MA inhibits autophagosome formation and CQ blocks autolysosome function, we concluded that MGF360-9L mediates autophagy-dependent degradation of DDX20. To further determine whether autophagy was involved in the degradation process, we examined initiation of autophagy by monitoring the conversion of microtubule-associated protein 1 light chain 3 (LC3)-I to LC3-II. HEK 293T cells were transfected with Flag-MGF360-9L plasmid for 24 h before immunoblot assays. As shown in Fig. 4H, overexpression of MGF360-9L significantly enhanced the LC3-II/LC3-I ratio in a dose-dependent manner. We next examined the formation and distribution of LC3 puncta using confocal microscopy. PK-15 cells were transfected with Myc-DDX20 plasmid alone or co-transfected with Flag-MGF360-9L and Myc-DDX20 plasmids for 24 h before IFA was performed. As shown in Fig. 4I, transfected DDX20 and GFP-LC3 were dispersed throughout the cytoplasm. Nevertheless, co-expression of MGF360-9L and DDX20 stimulated the formation of GFP-LC3 puncta and the colocalization of DDX20 with GFP-LC3. Taken together, these findings indicate that ASFV MGF360-9L mediates DDX20 degradation via the autophagy pathway.

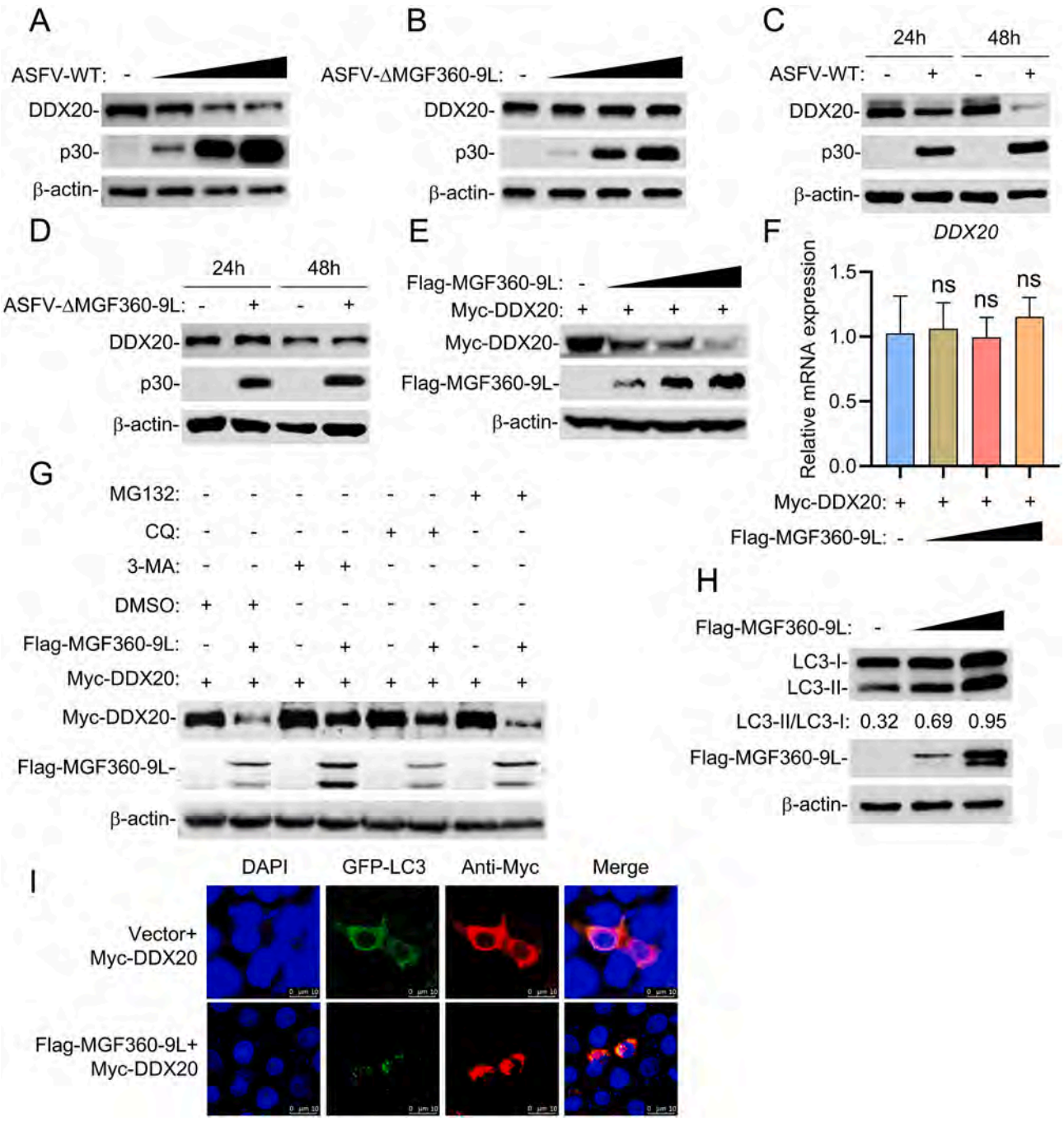

Fig. 4. MGF360-9L degrades DDX20 through autophagy pathway. **A, B** PAMs cultured in 12-well plates were infected with ASFV WT (**A**) or ASFV-ΔMGF360-9L (**B**) (MOI = 0, 0.1, 0.5, 1) for 24 h before immunoblot analysis. The production of DDX20, and p30 proteins was detected by Western blotting. β-actin was used as a loading control. **C, D** PAMs cultured in 12-well plates were uninfected or infected with ASFV WT (**C**) or ASFV-ΔMGF360-9 L (**D**) (MOI = 1) for 24 h and 48 h before immunoblot analysis. The production of DDX20, and p30 proteins was detected by Western blotting. β-actin was used as a loading control. **E, F** HEK 293T cells cultured in 12-well plates were co-transfected with Flag-MGF360-9L (0 μg/well, 0.5 μg/well, 1 μg/well, 2 μg/well) and Myc-DDX20 (1 μg/well) plasmids for 24 h before immunoblot (**E**) and qPCR experiments (**F**) were performed. **G** HEK 293T cells cultured in 12-well plates were co-transfected with empty vector (2 μg/well) or Flag-MGF360-9L (2 μg/well) and Myc-DDX20 (1 μg/well) plasmids. Eighteen hours later, cells were treated with DMSO, 3-MA (50 μM), CQ (100 μM) and MG132 (20 μM) for 6 h before immunoblot assays. **H** HEK 293T cells cultured in 12-well plates were transfected with Flag-MGF360-9L (0 μg/well, 0.5 μg/well, 1 μg/well) plasmid for 24 h before immunoblot assays. **I** PK-15 cells cultured in confocal dishes were co-transfected with GFP-LC3 (1 μg/well), Flag-MGF360-9L (1 μg/well) and Myc-DDX20 (1 μg/well) plasmids for 24 h. Cells were stained with anti-Myc antibody (red). Nuclei were stained with DAPI (blue). Scale bar = 10 μm. Data were analyzed by unpaired, two-tailed Student's *t*-test. Data are presented as the means ± SDs from three independent experiments. ns $P > 0.05$.

Rab1A promotes ASFV replication

Since previous studies have not reported that MGF360-9L can directly initiate the autophagy process, we speculated that MGF360-9L may be involved in DDX20 degradation by recruiting autophagy-related proteins. To test the hypothesis, we analyzed previous mass spectrometry data. The mass spectrometry results suggested that autophagy-related proteins including heat shock protein 70 (HSP70), heat shock protein 90 (HSP90), ATP binding cassette E1 (ABCE1), and Rab1A might be associated with MGF360-9L. To investigate which of

these proteins is exploited by MGF360-9L to degrade the antiviral protein DDX20, we first examined whether these proteins affect ASFV replication. As shown in Fig. 5A, MA104 cells were transfected with the indicated plasmids before ASFV infection. The qPCR results showed that overexpression of HSP70 and HSP90 had no obvious effect on the transcription of the ASFV *p30* gene. Notably, overexpression of ABCE1 and Rab1A, especially Rab1A, markedly promoted ASFV replication.

To explore the function of Rab1A in ASFV replication, MA104 cells were transfected with different doses of Myc-Rab1A plasmid for 24 h, followed by ASFV infection for another 24 h. Immunoblot assays showed that Rab1A overexpression facilitated the expression of ASFV p30 in a dose-dependent manner (Fig. 5B and C). Furthermore, MA104 cells were transfected with Myc-Rab1A plasmid and then infected with ASFV for another 24 h or 36 h. qPCR analysis showed that overexpression of Rab1A promoted the transcription of the ASFV *p30* gene post-infection (Fig. 5D). Consistently, as shown in Fig. 5E and F, overexpression of Rab1A enhanced ASFV p30 expression at the indicated time points during ASFV infection. To further investigate whether endogenous Rab1A is involved in ASFV replication, we designed siRNAs targeting Rab1A and down-regulated its expression (Fig. 5G–I). As shown in Fig. 5G, knockdown of Rab1A inhibited the transcription of the ASFV *p30* gene. Consistently, knockdown of Rab1A dramatically impaired the expression of ASFV p30 following viral infection (Fig. 5H and I). Taken together, these data suggest that Rab1A, an autophagy-related protein involved in MGF360-9L-mediated degradation of DDX20, promotes ASFV replication.

Rab1A, MGF360-9L and DDX20 form a complex

To examine whether Rab1A participates in the MGF360-9L-mediated degradation process, we first confirmed the interaction between Rab1A and MGF360-9L. HEK 293T cells were co-transfected with Flag-MGF360-9L and Myc-Rab1A expression plasmids for 24 h and then harvested for co-immunoprecipitation experiments. As shown in Fig. 6A and B, these results showed that Rab1A interacted with MGF360-9L. Similarly, as shown in Fig. 6C and D, co-immunoprecipitation assays indicated that Rab1A interacted with DDX20. The interaction among Rab1A, MGF360-9L and DDX20 was further confirmed by confocal microscopy. PK-15 cells were co-transfected with the indicated plasmids for 24 h before performing IFA. As shown in Fig. 6E and F, Rab1A colocalized with MGF360-9L and DDX20 in the cytoplasm. Since these three proteins interacted with each other, we next investigated whether Rab1A, MGF360-9L and DDX20 form a complex. As shown in Fig. 6G, co-immunoprecipitation experiments showed that Rab1A was associated with MGF360-9L and DDX20. In addition, Rab1A had no obvious effect on the association between MGF360-9L and DDX20 (Fig. 6G). Furthermore, GST pull-down assays showed that DDX20 directly bound to MGF360-9L and Rab1A (Fig. 6H). Taken together, these findings indicate that Rab1A is associated with MGF360-9L and DDX20, suggesting that Rab1A may be hijacked by MGF360-9L to facilitate the degradation of DDX20 during ASFV infection.

Rab1A participates in MGF360-9L-mediated autophagy degradation of DDX20

Previous studies have shown that Rab1A plays a crucial role in initiating autophagy processes and modulating the formation of autophagosomes (Webster et al., 2016; Jiang et al., 2023). We investigated whether Rab1A is exploited by MGF360-9L to participate in the autophagy-dependent degradation of DDX20. We first examined whether MGF360-9L affects the expression of Rab1A. HEK 293T cells were co-transfected with Myc-Rab1A and different doses of Flag-MGF360-9L expression plasmids for 24 h before immunoblot assays. As shown in Fig. 7A, MGF360-9L enhanced Rab1A expression in a dose-dependent manner. We next examined the effect of MGF360-9L on the expression of endogenous Rab1A. PAMs were infected with ASFV and ASFV-ΔMGF360-9L strain (MOI = 1) for the indicated time points. As shown in Fig. 7B, wild-type ASFV but not ASFV-ΔMGF360-9L infection induced the upregulation of endogenous Rab1A. These results indicated that MGF360-9L was responsible for promoting Rab1A expression. We further explored whether Rab1A affects the expression of DDX20. HEK 293T cells were co-transfected with HA-DDX20 and Myc-Rab1A expression plasmids for 24 h. Immunoblot assays showed that Rab1A promoted DDX20 degradation in a dose-dependent manner (Fig. 7C). Based on the above results, we assessed whether Rab1A affects MGF360-9L-mediated degradation of DDX20. HEK 293T cells were co-transfected with the indicated plasmids for 24 h. As shown in Fig. 7D, Rab1A and MGF360-9L synergistically promoted the degradation of DDX20.

To further corroborate the above conclusions, PAMs were transfected with the siRNAs targeting Rab1A for 36 h and then infected with ASFV for 24 h. As shown in Fig. 7E, the results indicated that Rab1A knockdown impaired ASFV-triggered degradation of endogenous DDX20. Furthermore, PK-15 cells were transfected with the siRNAs for 36 h and subsequently transfected with Flag-MGF360-9L plasmid for 24 h. The results showed that Rab1A knockdown attenuated MGF360-9L-mediated degradation of DDX20 (Fig. 7F). In the late phase of autophagy, autophagosomes generally fuse with lysosomes to form autolysosomes, thereby mediating the degradation of cargo proteins. Therefore, we investigated whether MGF360-9L is involved inregulating the above-mentioned process. As shown in Fig. 7G, co-transfected Rab1A and the lysosomal marker LAMP2A were mainly located in the perinuclear compartment. In contrast, MGF360-9L could promote cytoplasmic aggregation and more obvious co-localization of Rab1A and LAMP2A. These results showed that MGF360-9L facilitated the Rab1A-related autophagy degradation process. Collectively, these results suggest that Rab1A participates in MGF360-9L-mediated autophagy degradation of DDX20.

DISCUSSION

In the last decade, ASF has broken out around the world and continues to pose a significant threat to the pig industry. However, our knowledge of ASFV pathogenesis and virus-host interactions remains limited. As a tricky DNA virus, ASFV employs intricate factors for replication within the host, particularly by evading the host immune system through interactions with host proteins. Recently, several studies have highlighted the role of ASFV-encoded proteins in facilitating viral replication by destroying the host immune system. For instance, the ASFV virulence factor A137R negatively regulates the cGAS-STING-mediated IFN-β signaling pathway via autophagy-mediated lysosomal degradation of TBK1, thereby enhancing ASFV virulence (Sun et al., 2022). Furthermore, ASFV MGF300-2R inhibits host innate immune responses by mediating the autophagic degradation of IkappaB kinase alpha (IKKα) and IkappaB kinase beta (IKKβ) via the recruitment of toll interacting protein (TOLLIP) (Wang et al., 2023). In addition, ASFV MGF300-2R promotes ubiquitin-proteasome-mediated degradation of IKKβ with the assistance of the E3 ubiquitin ligase tripartite motif-containing protein 21 (TRIM21), contributing to viral immune evasion (Lu et al., 2024). It has been reported that MGF360-10L evades host innate immunity by recruiting the E3 ubiquitin ligase HECT domain- and RCC1-like domain-containing protein 5 (HERC5), which degrades the host protein JAK1 (Li et al., 2023,b). These ASFV-encoded proteins exert antagonistic functions through distinct mechanisms during different stages of ASFV infection, which highlights the diverse mechanisms strategies used by ASFV to evade host antiviral innate immunity and deepens our understanding of ASFV pathogenesis. Nevertheless, host factors can inhibit viral replication by regulating and degrading viral proteins. For example, the host protein 2′-5′-oligoadenylate synthetases 1 (OAS1) recruits the E3 ubiquitin ligase TRIM21 to degrade viral p72 protein, thereby inhibiting ASFV replication (Sun et al., 2023). Additionally, the host protein sorting

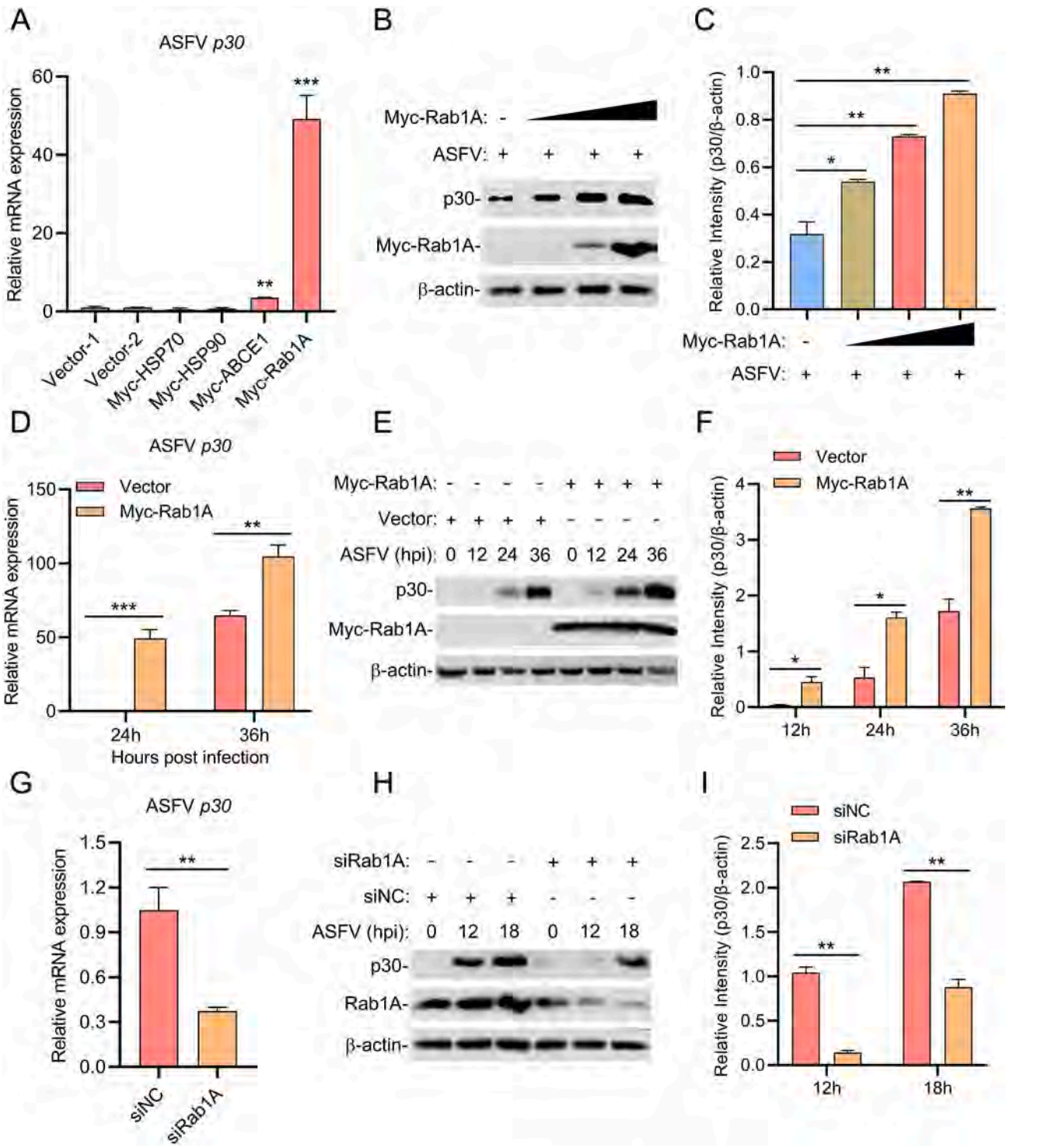

Fig. 5. Rab1A promotes ASFV replication. **A** MA104 cells cultured in 12-well plates were transfected with empty vector (1 μg/well), Myc-HSP70 (1 μg/well), Myc-HSP90 (1 μg/well), Myc-ABCE1 (1 μg/well) or Myc-Rab1A (1 μg/well) plasmid for 24 h before infected with ASFV (MOI = 1) for 24 h. The cells were subjected to qPCR experiments. **B, C** MA104 cells cultured in 12-well plates were transfected with Myc-Rab1A (0 μg/well, 0.5 μg/well, 1 μg/well, 2 μg/well) plasmid for 24 h and then infected with ASFV (MOI = 1) for 24 h before immunoblot assays. The relative intensity of p30 was standardized by β-actin and analyzed by Image J. **D** MA104 cells cultured in 12-well plates were transfected with Myc-Rab1A (1 μg/well) plasmid. Twenty-four hours later, cells were infected with ASFV (MOI = 1) for 24 h and 36 h before qPCR assays were performed. **E, F** MA104 cells cultured in 12-well plates were transfected with Myc-Rab1A (1 μg/well) plasmid. Twenty-four hours later, cells were infected with ASFV (MOI = 1) for 12 h, 24 h and 36 h before immunoblot assays were performed. The relative intensity of p30 was standardized by β-actin and analyzed by Image J. **G** PAMs cultured in 12-well plates were transfected with the indicated siRNAs (final concentration, 40 nM). Twenty-four hours later, cells were infected with ASFV (MOI = 1) for 24 h before qPCR experiments. **H, I** PAMs cultured in 12-well plates were transfected with the indicated siRNAs (final concentration, 40 nM). Twenty-four hours later, cells were infected with ASFV (MOI = 1) for 0 h, 12 h and 18 h before immunoblot assays. The relative intensity of p30 was standardized by β-actin and analyzed by Image J. Data were analyzed by unpaired, two-tailed Student's *t*-test. Data are presented as the means ± SDs from three independent experiments.*$P < 0.05$, **$P < 0.01$, ***$P < 0.001$.

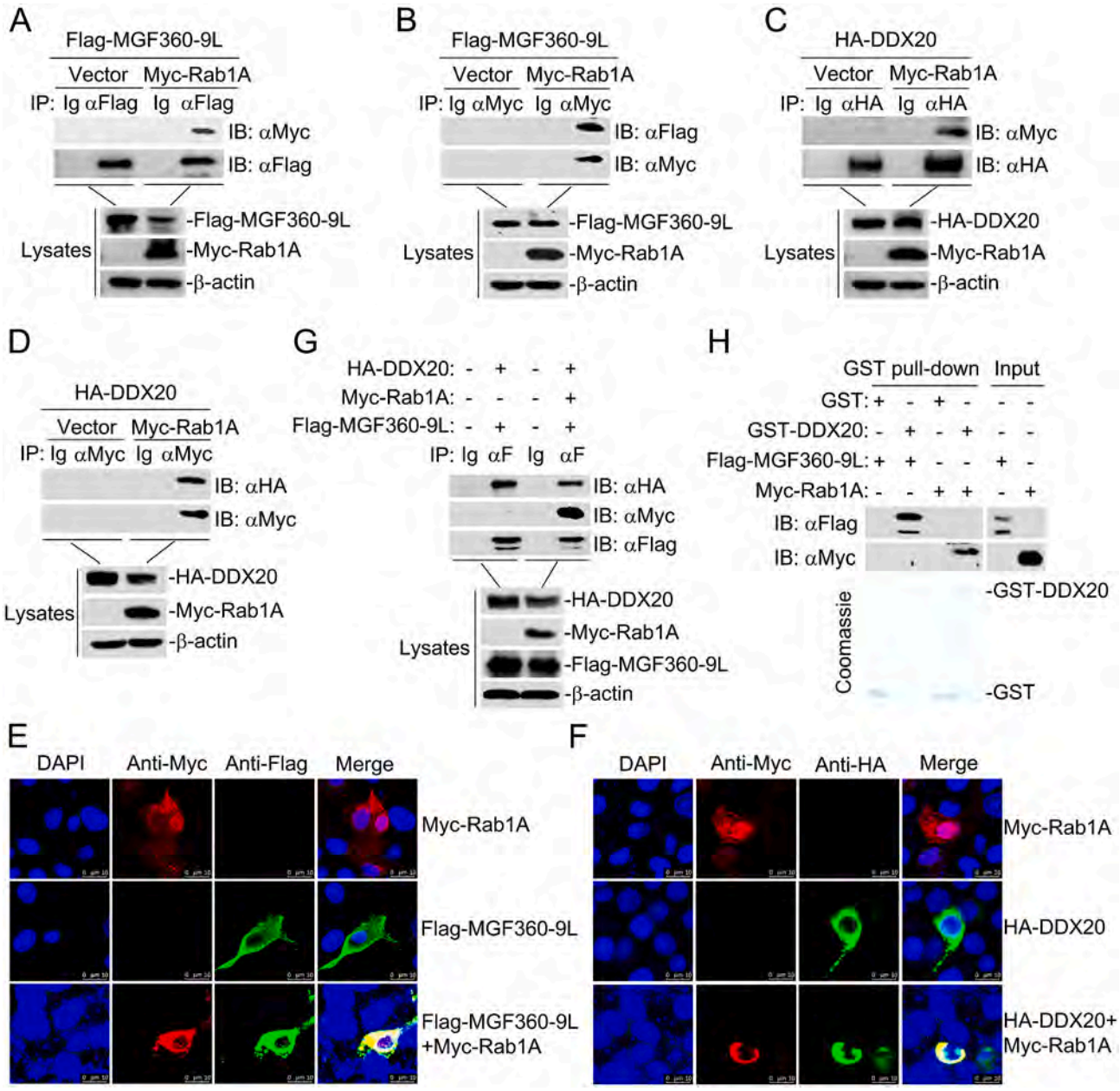

Fig. 6. Rab1A associates with MGF360-9L and DDX20. **A, B** HEK 293T cells cultured in 10 cm dishes were co-transfected with Flag-MGF360-9L (6 μg/dish) and Myc-Rab1A (6 μg/dish) plasmids for 24 h. Cell lysates were subjected to co-immunoprecipitation with anti-Flag antibody (**A**) or anti-Myc antibody (**B**) and immunoblot with the indicated antibodies. **C, D** HEK 293T cells cultured in 10 cm dishes were co-transfected with HA-DDX20 (6 μg/dish) and Myc-Rab1A (6 μg/dish) plasmids for 24 h. Cell lysates were subjected to co-immunoprecipitation with anti-HA antibody (**C**) or anti-Myc antibody (**D**) and immunoblot with the indicated antibodies. **E** PK-15 cells cultured in confocal dishes were co-transfected with Flag-MGF360-9L (2 μg/dish) and Myc-Rab1A (2 μg/dish) plasmids for 24 h. Cells were stained with anti-Flag antibody (green) and anti-Myc antibody (red). Nuclei were stained with DAPI (blue). Scale bar = 10 μm. **F** PK-15 cells cultured in confocal dishes were co-transfected with HA-DDX20 (2 μg/dish) and Myc-Rab1A (2 μg/dish) plasmids for 24 h. Cells were stained with anti-HA antibody (green) and anti-Myc antibody (red). Nuclei were stained with DAPI (blue). Scale bar = 10 μm. **G** HEK 293T cells cultured in 10 cm dishes were co-transfected with Flag-MGF360-9L (6 μg/dish), HA-DDX20 (6 μg/dish) and Myc-Rab1A (6 μg/dish) plasmids for 24 h. Cell lysates were subjected to co-immunoprecipitation with anti-Flag antibody and immunoblot with the indicated antibody. **H** HEK 293T cells cultured in 10 cm dishes were co-transfected with Flag-MGF360-9L (8 μg/dish) and Myc-Rab1A (8 μg/dish) plasmids for 24 h. Purified GST-DDX20 protein coupled to glutathione sepharose beads was incubated with the cell lysates for 3 h at 4 °C and then subjected to GST pull-down assays.

nexin 32 (SNX32), assisted by Ras-related protein Rab-1B (Rab1B) protein, degrades the viral p30 protein via the autophagy pathway, thereby inhibiting ASFV replication (Yang et al., 2024). The mechanism by which virulence factor MGF360-9L interacts with host proteins to regulate ASFV replication needs further investigation.

Elucidating the interaction between viruses and their hosts not only improves our understanding of viral pathogenesis, but also provides valuable insights for the development of antiviral therapies. Our previous studies have demonstrated that MGF360-9L plays a critical role in ASFV immune evasion. In this study, we first verified the association between MGF360-9L and host protein DDX20 using the interaction network of ASFV MGF360-9L with host proteins. Previous research has demonstrated that DDX20 interacts with two nucleoproteins of Epstein-Barr virus (EBV), namely EBNA2 and EBNA3C, to modulate the transcription of both viral and cellular genes (Styles et al., 2018). DDX20 has been shown to influence tumor development and progression, and its

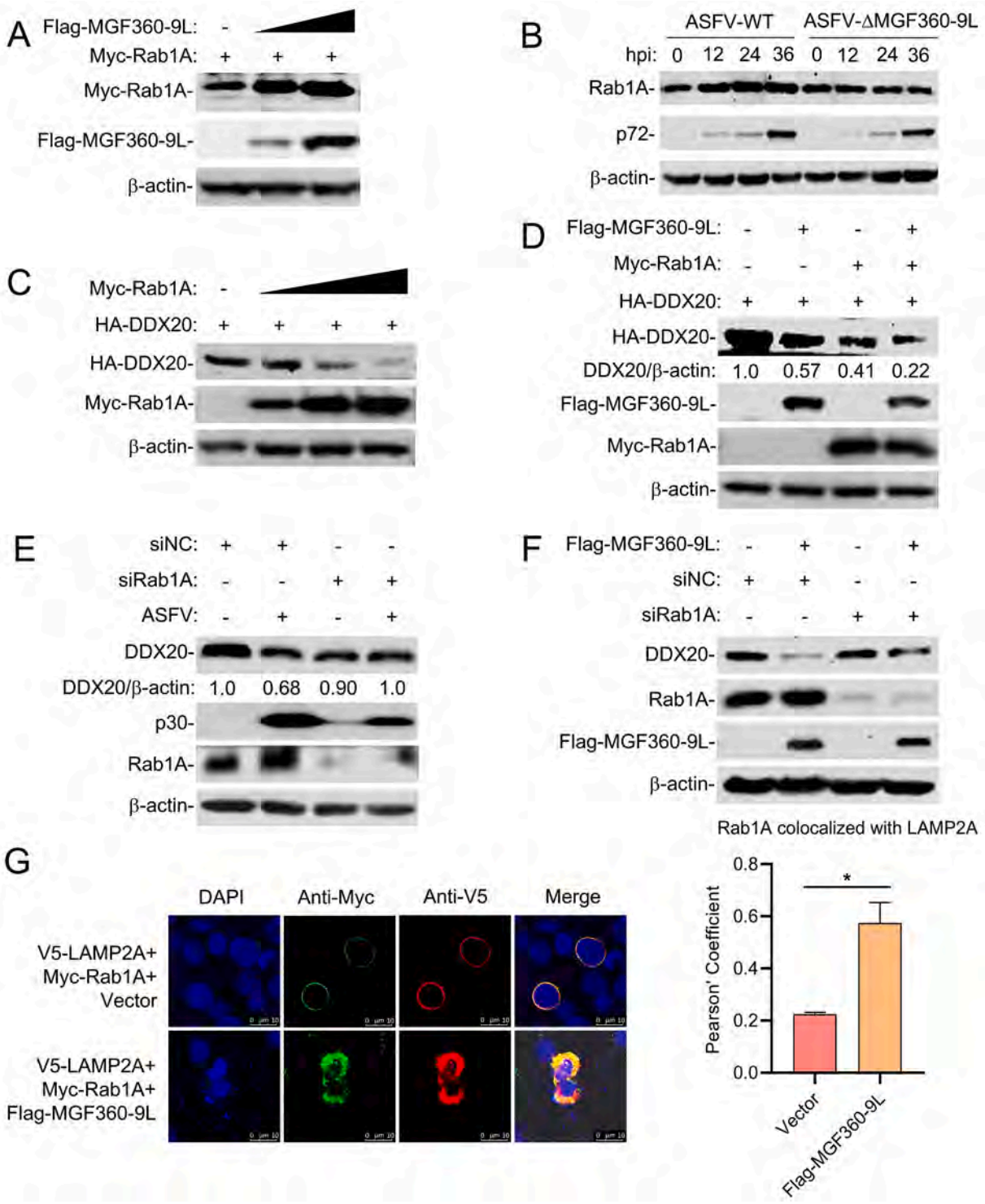

Fig. 7. Rab1A is involved in the ASFV MGF360-9L-mediated degradation of DDX20. **A** HEK 293T cells cultured in 12-well plates were co-transfected with Flag-MGF360-9L (0 μg/well, 0.5 μg/well, 1 μg/well) and Myc-Rab1A (1 μg/well) plasmids for 24 h before immunoblot assays were performed. **B** PAMs cultured in 12-well plates were uninfected or infected with ASFV-WT and ASFV-ΔMGF360-9L (MOI = 1) for 12 h, 24 h and 36 h before immunoblot assays were performed. **C** HEK 293T cells cultured in 12-well plates were co-transfected with Myc-Rab1A (0 μg/well, 0.5 μg/well, 1 μg/well, 2 μg/well) and HA-DDX20 (1 μg/well) plasmids for 24 h before immunoblot analysis. **D** HEK 293T cells cultured in 12-well plates were co-transfected with empty vector (2 μg/well), Flag-MGF360-9L (2 μg/well), Myc-Rab1A (2 μg/well) or HA-DDX20 (2 μg/well) plasmids for 24 h before immunoblot analysis. **E** PAMs cultured in 12-well plates were transfected with the indicated four siRNAs (final concentration, 40 nM). Twenty-four hours later, cells were infected with ASFV (MOI = 1) for 24 h before immunoblot experiments. **F** PK-15 cells cultured in 12-well plates were transfected with the indicated four siRNAs (final concentration, 40 nM) for 36 h. Then the cells were transfected with Flag-MGF360-9L (2 μg/well) and the empty vector (2 μg/well) for 24 h before immunoblot analysis. **G** PK-15 cells cultured in confocal dishes were co-transfected with Flag-MGF360-9L (1 μg/dish), Myc-Rab1A (1 μg/dish) and V5-LAMP2A (1 μg/dish) plasmids for 24 h. Cells were stained with anti-Myc antibody (green) and anti-V5 antibody (red). Nuclei were stained with DAPI (blue) (left). Scale bar = 10 μm. Quantitative analysis of colocalization of Rab1A with LAMP2A. Statistical analysis was based on colocalization images (covering dozens of cells) using the Image J (right). Graphs show mean ± SD (n = 12 cells from three individual images). Data are representative of at least two independent experiments with similar results. *$P < 0.05$ (unpaired, two-tailed Student's *t*-test).

functions exhibit considerable diversity. DDX20 not only promotes the progression of breast and prostate cancer by activating the DDX20-NF-κB-MMP9 axis, but also inhibits the NF-κB signaling pathway by employing distinct miRNAs, thereby acting as a tumor suppressor in liver cancer (Takata et al., 2011; Shin et al., 2014; Chen et al., 2016). The dual role of DDX20 in tumorigenesis makes it a promising target for drug development, and several anti-tumor agents that specifically target DDX20 have been designed. Up to now, the specific role of DDX20 during ASFV infection remains unclear. In this study, we found that DDX20 inhibits ASFV replication by positively regulating the IFN-I signaling pathway. Furthermore, ASFV MGF360-9L exploits Rab1A to promote DDX20 degradation through the autophagy pathway.

Overexpression of DDX20 dramatically inhibited ASFV replication, whereas knockdown of DDX20 had the opposite effect. The mechanism underlying this inhibition remains unclear. The interferon pathway plays a crucial role in the hos's innate immune response against viral infection. To investigate whether DDX20 inhibits ASFV replication by activating the interferon signaling pathway, we examined the effects of DDX20 on IFN-β promoter activation and the expression of downstream cytokines following ASFV infection. As expected, our findings confirmed that DDX20 activated the IFN-I signaling pathway to inhibit ASFV replication. A previous study has reported that DDX20 inhibits vesicular stomatitis virus (VSV) and herpes simplex virus-1 (HSV-1) replication by positively regulating the interferon pathway (Chen et al., 2024). It demonstrated that DDX20 promotes IRF3 phosphorylation and enhances the interaction between TBK1 and IRF3, thereby contributing to the expression of IFN-β. In this study, we found that DDX20 inhibited ASFV replication by promoting the activation of the IFN-I signaling. We speculated that DDX20 regulates ASFV replication through a similar mechanism. Therefore, we did not further investigate the detailed mechanism of DDX20-mediated activation of the IFN-I pathway during ASFV infection. DDX20 serves as an essential host restriction factor capable of combating ASFV infection. However, DDX20 expression was dramatically reduced following ASFV infection, suggesting that ASFV has evolved strategies to evade host defenses. Surprisingly, we found that ASFV-ΔMGF360-9L strain infection had no effect on DDX20 expression, indicating that MGF360-9L was involved in regulating DDX20 expression. Furthermore, overexpression of MGF360-9L induced DDX20 degradation in a dose-dependent manner. Two major pathways are responsible for intracellular protein degradation: the ubiquitin-proteasome system and the autophagy-lysosome pathway. To determine how MGF360-9L modulates DDX20 degradation, we used inhibitors targeting different degradation pathways and found that MGF360-9L mediated DDX20 degradation via the autophagy pathway, however, the underlying mechanisms remains to be elucidated.

Autophagy is a lysosomal degradation pathway that plays a crucial role in various aspects of immunity, including the development of the immune system, the regulation of immune and inflammatory responses, the selective degradation of intracellular microorganisms, and the host's response to infectious diseases (Glick et al., 2010; Levine et al., 2011). Many viral proteins typically recruit membrane transport proteins to facilitate the degradation of host proteins, thereby enhancing viral replication and immune evasion. For instance, the E protein of porcine reproductive and respiratory syndrome virus (PRRSV) degrades DEAD/H-box RNA helicase 10 (DDX10) via SQSTM1/p62-dependent selective autophagy, thereby antagonizing its antiviral activity (Li et al., 2023). Rab1A is a member of the Rab GTPase family with a molecular weight of 23.5 kDa. Previous studies have demonstrated that Rab1A is primarily localized in the endoplasmic reticulum and Golgi apparatus, where it facilitates the transport of vesicles from the endoplasmic reticulum to the Golgi apparatus (Stenmark, 2009). Increasing evidence indicates that Rab1A plays a significant role in autophagy regulation, particularly by influencing vesicle formation and trafficking. It mediates the trafficking of ULK1 complexes to phagosomes and is also involved in the delivery of Atg9-positive membranes to the phagosome (Webster et al., 2016). Moreover, Rab1A also plays extensive roles in regulating multiple virus replication. Research indicates that autophagy, triggered by the interaction between Rab1A and ULK1, facilitates the replication of PRRSV (Jiang et al., 2023). RAB1A interacts with C9orf72 to induce ULK1-mediated autophagy, thereby promoting hepatitis B virus (HBV) replication (Li et al., 2025). Collectively, the Rab1A-mediated autophagy process can be exploited by multiple viruses to escape host immune surveillance and facilitate viral replication, which provides new insights into the development of broad-spectrum anti-viral strategies.

In this study, we found that Rab1A interacted with MGF360-9L, as indicated by mass spectrometry data. This led us to speculate that MGF360-9L regulated the autophagy process by interacting with Rab1A. However, the role of Rab1A during ASFV replication remain enigmatic. Endogenous Rab1A was induced following ASFV infection, and MGF360-9L was responsible for this increase. We found that overexpression of Rab1A could enhance ASFV replication, whereas knockdown of Rab1A had the opposite effect. To determine whether MGF360-9L-mediated degradation of DDX20 is dependent on Rab1A, we performed the corresponding experiments and demonstrated that Rab1A induced DDX20 degradation in a dose-dependent manner. Similarly, Rab1A deficiency significantly impaired MGF360-9L-mediated degradation of DDX20. These findings indicate that MGF360-9L recruits Rab1A to promote DDX20 degradation via the autophagy pathway during ASFV infection. Taken together, Rab1A can be hijacked by multiple viruses to facilitate efficient replication, making it a promising target for broad-spectrum antiviral therapies.

CONCLUSIONS

In summary, our findings demonstrate that the virulence factor MGF360-9L recruits the autophagy-related protein Rab1A to degrade the antiviral protein DDX20, thereby promoting ASFV replication. Overall, this study significantly broadens our understanding of the sophisticated regulatory network between ASFV virulence factors and host systems, identifies potential targets for the development of antiviral drugs, and provides a theoretical foundation for further investigation into the pathogenesis and immune evasion mechanisms of ASFV.

MATERIALS AND METHODS

Cells and viruses

HEK 293T, PK-15 and MA104 cells were obtained from a Chinese culture center and cultured in DMEM (Dulbecco's Modified Eagle Medium; Gibco, China) supplemented with 10% fetal bovine serum (FBS; Gibco, New Zealand), along with 1% penicillin and 1% streptomycin (Gibco, United States). PAMs were prepared as previously described and cultured in RPMI 1640 medium (Thermo Scientific, USA) supplemented with 10% fetal calf serum (Carrascosa et al., 1982). All cells were maintained at 37 °C in the 5% CO_2 atmosphere. The parental ASFV strain (ASFV WT, CN/GS/2018) and the *MGF360-9L* gene-deleted ASFV strain (ASFV ΔMGF360-9L) were provided by the Lanzhou Veterinary Research Institute, Chinese Academy of Agricultural Sciences. All ASFV experiments were conducted in the Biosafety Level 3 Laboratory (BSL-3) at the Lanzhou Veterinary Research Institute, strictly adhering to the recommendations outlined in the “Guidelines for the Care and Use of Laboratory Animals” issued by the Ministry of Science and Technology of the People's Republic of China.

Plasmids, antibodies, and reagents

The ORF of MGF360-9L was amplified from the genome of the parental ASFV WT strain and subsequently cloned into the pCDNA3.1 vector, incorporating either a Flag or EGFP tag. The DDX20 related plasmids and Rab1A related plasmids were cloned into the pCDNA3.1

vector by standard molecular clone methods. The LAMP2A plasmid was cloned into the pCDNA3.4 vector by standard molecular clone methods. The plasmids pIFN-β-luc, and pRL-TK were all prepared in our laboratory prior to the experiments.

Mouse anti-p72 (B646L) and mouse anti-p30 (CP204L) monoclonal antibodies were prepared in our laboratory. Additionally, rabbit polyclonal anti-DDX20 (11324-1-AP), rabbit polyclonal anti-Rab1A (11671-1-AP), horseradish peroxidase (HRP)-conjugated goat anti-rabbit IgG (H + L; SA00001-2), enzyme-labeled goat anti-mouse IgG (H + L; SA00001-1), mouse anti-β-actin monoclonal antibody (66,009-1-Ig), and mouse anti-GFP monoclonal antibody (66,002-1-Ig) were procured from Proteintech, Wuhan, China. Mouse monoclonal anti-Myc (2276S), rabbit monoclonal anti-Flag (14793S), rabbit monoclonal anti-HA (3724S), anti-rabbit IgG (H + L) F(ab') fragment conjugated to Alexa Fluor 488 (4412S), and anti-mouse IgG (H + L) F(ab')2 fragment conjugated to Alexa Fluor 594 (8890S) antibodies were obtained from Cell Signaling Technology (Danvers, MA, USA). The Rabbit MGF360-9L polyclonal antibody was prepared in our laboratory.

Protein G Sepharose (17061801) was sourced from GE Healthcare Biosciences AB (Pittsburgh, PA, USA). 3-Methyladenine (3-MA) (S2767) was purchased from Selleck (Shanghai, China), MG132 (T2154) and chloroquine (CQ) (T8689) were purchased from TargetMol (Shanghai, China). The jetPRIME transfection reagent (PT-114-15) was acquired from Polyplus-Transfection SA (Strasbourg, France). Poly (dA: dT) (Cat# tlrl-patn) was purchased from InvivoGen (Shanghai, China).

RNA interference

The siRNA targeting DDX20 and Rab1A were synthesized by GenePharma (Shanghai, China). The cells were transfected with siRNA by using PepMute siRNA transfection reagent (SignaGen Laboratories) according to the manufacturer's instructions. The sequences of each siRNA are as follows: siDDX20-1: CACGUUUGUAAGACUAAAUTT, siDDX20-2: GUGGCUUCAUCAAGAAAUATT, siDDX20-3: CCCGGAGCAAAGGAAAUAATT, siDDX20-4: GCCUCUCAGUCGUAUUACUTT; siRab1A-1: AAGCUAUAUCAGCACAAUUTT, siRab1A-2: GAACAAUCACCUCCAGUUATT, siRab1A-3: GAUCGUUAUGCCAGUGAAATT, siRab1A-4: ACGAAUGUAGAACAGUCUUTT.

Co-immunoprecipitation and immunoblot analysis

For co-immunoprecipitation experiments, HEK 293T and PK-15 cells were transfected with indicated plasmids for 24 h. The cells were harvested and lysed in 1 mL NP-40 lysis buffer composed of 20 mM Tris-HCl (pH 7.5), 150 mM NaCl, 1% NP-40, 1 mM EDTA, and the protease inhibitor cocktail. For each immunoprecipitation, 0.4 mL of cell lysate was incubated with 0.5 μg of the indicated antibody or control IgG and 50 μL Protein G Sepharose beads (GE Healthcare) at 4 °C for 4 h. The beads were added with 50 μL 2 × SDS loading buffer and boiled for 10 min before SDS-PAGE. Immunoblot was performed according to standard procedures.

GST-pull down and immunoblot analysis

GST-DDX20 protein was purified with glutathione sepharose. HEK 293T cells were transfected with Flag-MGF360-9L and Myc-Rab1A plasmids for 24 h. The cell lysates were then added to the purified recombinant GST-DDX20 protein coupled to glutathione sepharose beads and incubated for 3 h at 4 °C. Subsequently, the beads were washed and boiled. The inputs were fractionated by SDS-PAGE and detected by Coomassie staining or immunoblot analysis.

Indirect immunofluorescence assay (IFA)

HEK 293T and PK-15 cells were transfected with the indicated plasmids for 24 h. The cells were washed three times with pre-chilled PBS and then fixed with 4% paraformaldehyde for 30 min. Following fixation, the cells were treated with PBS containing 0.3% Triton X-100 for 10 min at room temperature. Subsequently, the cells were blocked with 5% bovine serum albumin for 1 h at room temperature. Then the cells were incubated overnight at 4 °C with specific antibodies against Flag, Myc, HA, which were diluted in PBS with 1% bovine serum albumin and 0.3% Triton X-100. After three washes with pre-chilled PBST, the cells are incubated with fluorescein-labeled antibodies (Alexa 488 anti-rabbit and Alexa 594 anti-mouse) at room temperature for 1 h. After washing with PBST, the cells were stained with diluted DAPI for 10 min at room temperature before being observed by laser-scanning confocal microscopy (LSCM, Leica SP8, Solms, Germany). ImageJ v1.8.0 software, Coloc 2 plugin and Costes algorithm were used to determine the Pearson's coefficient.

Luciferase reporter assays

HEK 293T and MA104 cells were cultured on 24-well plate. The cells were transfected with the indicated plasmids or infected with ASFV. The pRL-TK reporter plasmid was utilized as the internal reference gene. Luciferase assays were performed using a dual-specific luciferase assay kit (Promega). Firefly luciferase activities were normalized on the basis of Renilla luciferase activities.

RNA extraction and RT-qPCR

Total RNA was extracted from PAMs, HEK 293T cells, and MA104 cells following the manufacturer's standard TRIzoL reagent extraction protocol (ThermoFisher Scientific, 15596018). The PrimeScriptTM RT reagent Kit with gDNA Eraser (Takara Bio Inc, RR047A) was utilized according to the provided instructions. The extracted total RNA was reverse transcribed, and the resulting cDNA was subjected to quantitative real-time PCR (qPCR) using Power Up SYBR Green Master Mix on the ABI StepOnePlus system. All data obtained were analyzed using StepOnePlus software, with mRNA levels normalized to GAPDH of the same species as the standard. The relative mRNA expression was calculated and compared using the cycle threshold ($2^{-\Delta\Delta Ct}$) method. The sequences of all primers used in this study were presented in Supplementary Table S1.

Statistical analysis

All experiments were conducted independently three times, and statistical analyses was determined using an unpaired two-tailed Student's *t*-test. $P < 0.05$ indicated that the difference was statistically significant (ns $P > 0.05$; $^{*}P < 0.05$; $^{**}P < 0.01$; $^{***}P < 0.001$; $^{****}P < 0.0001$).

DATA AVAILABILITY

The authors confirm that the data supporting the findings of this study are available within the article.

ETHICS STATEMENT

This article does not contain any studies with human or animal subjects performed by any of the authors.

AUTHOR CONTRIBUTIONS

Lu He: conceptualization, data curation, investigation, writing & original draft, writing – review & editing. Xuxu Fan: data curation, formal analysis, methodology, writing & original draft, writing – review & editing. Zhaoyu Zhu: investigation, methodology. Danshi Pei: investigation, methodology. Yizhuo Wang: investigation, methodology. Xizhong Li: investigation, methodology. Qingfeng Ren: investigation,

methodology. Haixue Zheng, Weiwei Li and Zixiang Zhu: investigation, methodology, project administration, writing-review & editing, funding acquisition, supervision.

CONFLICT OF INTEREST

The authors declare that they have no conflict of interest. Prof. Haixue Zheng is an editorial board member for *Virologica Sinica* and was not involved in the editorial review or the decision to publish this article.

ACKNOWLEDGEMENTS

This work was supported by the grants from the open competition program of top ten critical priorities of Agricultural Science and Technology Innovation for the 14th Five-Year Plan of Guangdong Province (2024KJ14), the Fundamental Research Funds for the Central Universities (lzujbky-2022-ct02), the Project of National Center of Technology Innovation for Pigs (NCTIP-XD/C03), the Youth Innovation Program of the Chinese Academy of Agricultural Sciences (Y2025QC33), the Major Science and Technology Project of Gansu Province (22ZD6NA001 and 22ZD6NA012), the Innovation Program of Chinese Academy of Agricultural Sciences (CAAS-CSLPDCP-2023002 and CAAS-ASTIP-2025-LVRI), the China Postdoctoral Science Foundation (2023M743830), the Earmarked Fund for CARS-35 and CARS-39-13, and the Fundamental Research Funds for Innovation Team of Gansu Province (23JRRA546, 23JRRA548), and the Basic Scientific Research Fund of LVRI (1610312021009).

APPENDIX A. SUPPLEMENTARY DATA

Supplementary data to this article can be found online at https://doi.org/10.1016/j.virs.2025.10.001.

REFERENCES

Afonso, C.L., Piccone, M.E., Zaffuto, K.M., Neilan, J., Kutish, G.F., Lu, Z., Balinsky, C.A., Gibb, T.R., Bean, T.J., Zsak, L., Rock, D.L., 2004. African swine fever virus multigene family 360 and 530 genes affect host interferon response. J. Virol. 78, 1858–1864.

Alejo, A., Andrés, G., Salas, M.L., 2003. African Swine Fever virus proteinase is essential for core maturation and infectivity. J. Virol. 77, 5571–5577.

Ali, M.a.M., 2021. DEAD-box RNA helicases: the driving forces behind RNA metabolism at the crossroad of viral replication and antiviral innate immunity. Virus Res. 296, 198352.

Cai, Q., Guo, Y., Xiao, B., Banerjee, S., Saha, A., Lu, J., Glisovic, T., Robertson, E.S., 2011. Epstein-Barr virus nuclear antigen 3C stabilizes Gemin3 to block p53-mediated apoptosis. PLoS Pathog. 7, e1002418.

Carrascosa, A.L., Santarén, J.F., Viñuela, E., 1982. Production and titration of African swine fever virus in porcine alveolar macrophages. J. Virol. Methods 3, 303–310.

Chen, W., Zhou, P., Li, X., 2016. High expression of DDX20 enhances the proliferation and metastatic potential of prostate cancer cells through the NF-κB pathway. Int. J. Mol. Med. 37, 1551–1557.

Chen, Z., Zhang, J., Feng, T., Wang, X., Zhou, S., Pan, W., Chen, Z., Yan, Y., Dai, J., 2024. DDX20 positively regulates the interferon pathway to inhibit viral infection. Antivir. Res. 225, 105875.

Curmi, F., Cauchi, R.J., 2018. The multiple lives of DEAD-box RNA helicase DP103/DDX20/Gemin3. Biochem. Soc. Trans. 46, 329–341.

De Villiers, E.P., Gallardo, C., Arias, M., Da Silva, M., Upton, C., Martin, R., Bishop, R.P., 2010. Phylogenomic analysis of 11 complete African swine fever virus genome sequences. Virology 400, 128–136.

Gao, Q., Yang, Y., Quan, W., Zheng, J., Luo, Y., Wang, H., Chen, X., Huang, Z., Chen, X., Xu, R., Zhang, G., Gong, L., 2021. The African swine fever virus with MGF360 and MGF505 deleted reduces the apoptosis of porcine alveolar macrophages by inhibiting the NF-κB signaling pathway and Interleukin-1β. Vaccines (Basel) 9, 1371.

Glick, D., Barth, S., Macleod, K.F., 2010. Autophagy: cellular and molecular mechanisms. J. Pathol. 221, 3–12.

He, L., Yang, J., Hao, Y., Yang, X., Shi, X., Zhang, D., Zhao, D., Yan, W., Bie, X., Chen, L., Chen, G., Zhao, S., Liu, X., Zheng, H., Zhang, K., 2023. DDX20: a multifunctional complex protein. Molecules 28, 7198.

Huang, H., Dang, W., Shi, Z., Ding, M., Xu, F., Li, T., Feng, T., Zheng, H., Xiao, S., 2023. Identification of African swine fever virus MGF505-2R as a potent inhibitor of innate immunity in vitro. Virol. Sin. 38, 84–95.

Jiang, C., Diao, F., Ma, Z., Zhang, J., Bai, J., Nauwynck, H., Jiang, P., Liu, X., 2023. Autophagy induced by Rab1a-ULK1 interaction promotes porcine reproductive and respiratory syndrome virus replication. Virus Res. 323, 198989.

Karger, A., Pérez-Núñez, D., Urquiza, J., Hinojar, P., Alonso, C., Freitas, F., Revilla, Y., Le Potier, M.-F., Montoya, M., 2019. An update on African swine fever virology. Viruses 11, 864.

Levine, B., Mizushima, N., Virgin, H.W., 2011. Autophagy in immunity and inflammation. Nature 469, 323–335.

Li, C., Zhao, Z., Guo, B., Xu, D., Li, S., Tang, H., Jia, B., Li, F., Zhang, J., Zou, H., Lu, M., Huang, A., Lin, Y., 2025. RAB1A promotes hepatitis B virus replication by enhancing PPARα-mediated viral transcription and inducing ULK1-mediated autophagy. Int. J. Biol. Macromol. 321, 146301.

Li, D., Peng, J., Wu, J., Yi, J., Wu, P., Qi, X., Ren, J., Peng, G., Duan, X., Ru, Y., Liu, H., Tian, H., Zheng, H., 2023. African swine fever virus MGF-360-10L is a novel and crucial virulence factor that mediates ubiquitination and degradation of JAK1 by recruiting the E3 ubiquitin ligase HERC5. mBio 14, e0060623.

Li, J., Zhou, Y., Zhao, W., Liu, J., Ullah, R., Fang, P., Fang, L., Xiao, S., 2023. Porcine reproductive and respiratory syndrome virus degrades DDX10 via SQSTM1/p62-dependent selective autophagy to antagonize its antiviral activity. Autophagy 19, 2257–2274.

Lu, Z., Luo, R., Lan, J., Chen, S., Qiu, H.-J., Wang, T., Sun, Y., 2024. In: The MGF300-2R Protein of African Swine Fever Virus Promotes IKKβ Ubiquitination by Recruiting the E3 Ubiquitin Ligase TRIM21. Viruses 16, 949.

O'donnell, V., Holinka, L.G., Gladue, D.P., Sanford, B., Krug, P.W., Lu, X., Arzt, J., Reese, B., Carrillo, C., Risatti, G.R., Borca, M.V., 2015. African swine fever virus Georgia isolate harboring deletions of MGF360 and MGF505 genes is attenuated in swine and confers protection against challenge with virulent parental virus. J. Virol. 89, 6048–6056.

Rathakrishnan, A., Connell, S., Petrovan, V., Moffat, K., Goatley, L.C., Jabbar, T., Sánchez-Cordón, P.J., Reis, A.L., Dixon, L.K., 2022. Differential effect of deleting members of African swine fever virus multigene families 360 and 505 from the genotype II Georgia 2007/1 isolate on virus replication, virulence, and induction of protection. J. Virol. 96, e0189921.

Reis, A.L., Netherton, C., Dixon, L.K., 2017. Unraveling the armor of a killer: evasion of host defenses by African swine fever virus. J. Virol. 91, 2338, 02316.

Shin, E.M., Hay, H.S., Lee, M.H., Goh, J.N., Tan, T.Z., Sen, Y.P., Lim, S.W., Yousef, E.M., Ong, H.T., Thike, A.A., et al., 2014. DEAD-box helicase DP103 defines metastatic potential of human breast cancers. J. Clin. Investig. 124, 3807–3824.

Stenmark, H., 2009. Rab GTPases as coordinators of vesicle traffic. Nat. Rev. Mol. Cell Biol. 10, 513–525.

Styles, C., Paschos, K., White, R., Farrell, P., 2018. The cooperative functions of the EBNA3 proteins are central to EBV persistence and latency. Pathogens 7, 31.

Sun, H., Wu, M., Zhang, Z., Wang, Y., Yang, J., Liu, Z., Guan, G., Luo, J., Yin, H., Niu, Q., 2023. OAS1 Suppresses African Swine Fever Virus Replication by Recruiting TRIM21 to Degrade Viral Major Capsid Protein, 97, e01217-01223.

Sun, M., Yu, S., Ge, H., Wang, T., Li, Y., Zhou, P., Pan, L., Han, Y., Yang, Y., Sun, Y., Li, S., Li, L.F., Qiu, H.J., 2022. The A137R protein of African swine fever virus inhibits type I interferon production via the autophagy-mediated lysosomal degradation of TBK1. J. Virol. 96, e0195721.

Takata, A., Otsuka, M., Kojima, K., Yoshikawa, T., Kishikawa, T., Yoshida, H., Koike, K., 2011. MicroRNA-22 and microRNA-140 suppress NF-κB activity by regulating the expression of NF-κB coactivators. Biochem. Biophys. Res. Commun. 411, 826–831.

Wang, G., Xie, M., Wu, W., Chen, Z., 2021. Structures and functional diversities of ASFV proteins. Viruses 13, 2124.

Wang, T., Luo, R., Zhang, J., Lu, Z., Li, L.F., Zheng, Y.H., Pan, L., Lan, J., Zhai, H., Huang, S., Sun, Y., Qiu, H.J., 2023. The MGF300-2R protein of African swine fever virus is associated with viral pathogenicity by promoting the autophagic degradation of IKKα and IKKβ through the recruitment of TOLLIP. PLoS Pathog. 19, e1011580.

Webster, C.P., Smith, E.F., Bauer, C.S., Moller, A., Hautbergue, G.M., Ferraiuolo, L., Myszczynska, M.A., Higginbottom, A., Walsh, M.J., Whitworth, A.J., Kaspar, B.K., Meyer, K., Shaw, P.J., Grierson, A.J., De Vos, K.J., 2016. The C9orf72 protein interacts with Rab1a and the ULK1 complex to regulate initiation of autophagy. EMBO J. 35, 1656–1676.

Yang, B., Zhang, D., Shi, X., Shen, C., Hao, Y., Zhang, T., Yang, J., Yuan, X., Chen, X., Zhao, D., Cui, H., Li, D., Zhu, Z., Tian, H., Yang, F., Zheng, H., Zhang, K., Liu, X., 2021. Construction, identification and analysis of the interaction network of African swine fever virus MGF360-9L with host proteins. Viruses 13, 1804.

Yang, W., Li, L., Zhang, J., Wu, J., Kang, W., Wang, Y., Ding, H., Li, D., Zheng, H., 2024. SNX32 is a Host Restriction Factor that Degrades African Swine Fever Virus CP204L via the RAB1B-dependent Autophagy Pathway, 98, e01599-01523.

Yozawa, T., Kutish, G.F., Afonso, C.L., Lu, Z., Rock, D.L., 1994. Two novel multigene families, 530 and 300, in the terminal variable regions of African swine fever virus genome. Virology 202, 997–1002.

Zhang, K., Yang, B., Shen, C., Zhang, T., Hao, Y., Zhang, D., Liu, H., Shi, X., Li, G., Yang, J., et al., 2022. MGF360-9L is a major virulence factor associated with the African swine fever virus by antagonizing the JAK/STAT signaling pathway. mBio 13, e0233021.

Zhou, X., Li, N., Luo, Y., Liu, Y., Miao, F., Chen, T., Zhang, S., Cao, P., Li, X., Tian, K., Qiu, H.J., Hu, R., 2018. Emergence of African Swine Fever in China, 2018. Transbound. Emerg. Dis. 65, 1482–1484.

Zsak, L., Lu, Z., Burrage, T.G., Neilan, J.G., Kutish, G.F., Moore, D.M., Rock, D.L., 2001. African swine fever virus multigene family 360 and 530 genes are novel macrophage host range determinants. J. Virol. 75, 3066–3076.